RSC Advances

RSC Publishing

PAPER

View Article Online
View Journal | View Issue

Cite this: *RSC Advances*, 2013, **3**, 5649

Uniform double-shelled silica hollow spheres: acid/base selective-etching synthesis and their drug delivery application

Longfei Tan,[a] Tianlong Liu,[a] Linlin Li,[a] Huiyu Liu,[a] Xiaoli Wu,[ac] Fuping Gao,[a] Xiaolong He,[ac] Xianwei Meng,[a] Dong Chen*[b] and Fangqiong Tang*[a]

Received 16th January 2013,
Accepted 12th February 2013

DOI: 10.1039/c3ra40733k

www.rsc.org/advances

Uniform mono-disperse double-shelled silica hollow spheres (DSH) with controllable inner structure have been successfully synthesized *via* an alternating acid/base selective etching strategy. The void spacing between the shells can be tuned during the synthesis. The formation mechanism was proposed by monitoring the synthesis process at different reaction time and comparative investigation of the used surfactants. Anti-cancer drug, mitoxantrone (Mito) was chosen as a probing molecule in drug delivery and release experiments, and the results showed that these double-shelled silica hollow spheres exhibit higher drug loading capacity and desired release rates compared with conventional single-shelled silica hollow spheres due to their hierarchically mesoporous structures. The *in vitro* cellular internalization of DSH was evaluated by designing fluorescein isothiocyanate labeled DSH with green fluorescence (DSH@FITC). The *in vitro* study of Human liver carcinoma cells of Hep-G2 cells also proves that the DSH–Mito has reduced toxicity and enhanced therapeutic efficacy, and the DSH is an ideal carrier for drug delivery.

Introduction

Precisely regulating the fine structure of nanomaterials has been pursued year by year due to their great influence on their application in catalysis, drug delivery and energy storage. Hollow/rattle-type nanostructures with interstitial hollow space and mesoporous shell have low density, high specific area and highly permeable porous shell for the penetrating of guest species, which are ideal for drug carriers, catalyst support and electrodes materials.[1–7] Recently, the synthesis of multi-shelled hollow/rattle-type nanostructures has made tremendous advances because of their potential advantages, such as prolonging the release of guest species in drug delivery and improving the energy conversion efficiency in lithium batteries and solar cells.[8–13]

Due to their biocompatibility, low toxicity, high chemical and mechanical stabilities, silica hollow spheres with multi-shells have show great potential in drug delivery application. Few synthesis approaches have been developed, such as self-template method, soft template method and selective etching strategy.[14–19] Yin *et al.* demonstrated a ''surface-protected etching'' self-templated method for the synthesis of hollow nanospheres with double shell.[14] Yeh *et al.* built multi-shelled mesoporous silica by a self-templated synthesis involving interior channel wall and outermost surface protection.[15] Qiao *et al.* synthesized multi-shelled mesoporous silica hollow nanospheres through a facile vesicle template approach derived from a self-assembly of surfactants.[17] Self-templated and soft template methods are effective for the synthesis of hollow/rattle-type nanomaterials, but it is difficult to fabricate nanospheres with good dispersity and to control the particle size, and shell thickness. For the size and shape of nanoparticles have important impacts on their fates in organisms, the lack of uniform and monodispersity is a barrier to investigate the drug loading and release efficiency of silica hollow spheres as effective drug carriers.[20–22]

Li *et al.* reported a selective etching strategy to fabricate double-shelled silica hollow microspheres. They first prepared penta-layer alternating silica/polymer hybrid microspheres *via* combined inorganic sol–gel reaction and distillation–precipitation polymerization, and then calcined the alternating PMAA layers to obtain double-shelled silica hollow microspheres.[18] However, polymerization and cross-linking of the PMAA is complicated. The calcination process usually make microspheres difficult to re-disperse in water. Although some works have been reported to synthesis silica hollow spheres with double shell, it still needs an effective strategy to synthesize the highly uniform mono-disperse hollow spheres with controllable shells and inner structure. With the void space between the shells ideally suited to load guest species and

[a]*Laboratory of Controllable Preparation and Application of Nanomaterials, Technical Institute of Physics and Chemistry, Chinese Academy of Sciences, Beijing 100190, P. R. China. E-mail: tangfq@mail.ipc.ac.cn; Tel: +86-10-82543521*
[b]*Beijing Creative Nanophase Hi-Tech Company, Limited, Beijing, 100086, P. R. China. E-mail: creative.nanophase@gmail.com*
[c]*University of the Chinese Academy of Sciences, Beijing, 100049, P. R. China*

determine the transport of functional molecules in and out of the voids, to control the space between the shells and inner cavity is also of great importance.

Recently, our group elaborately fabricated an organic–inorganic hybrid silica sphere with a three-layer ''sandwich'' structure. The silica hollow spheres with single shell were successfully prepared by etching the middle layer, which condensed from N-[3-(trimethoxysilyl) propyl] ethylenediamine (TSD) and tetraethylorthosilane (TEOS).[23] Because their mesoporous shell and interstitial hollow space can selectively and efficiently load drug molecules, these silica nanorattles have great potential for high drug loading efficiencies. Our previous work have proved that the silica hollow spheres with single shell can act as a versatile carrier for the delivery of hydrophobic anti-cancer drug, docetaxel, and hydrophilic anti-cancer drugs, doxorubicin.[24–26] For the purpose of increasing drug loading capacity and release behavior, herein, we further explore an alternating acid/base selective etching strategy to synthesis highly uniform mono-disperse double-shelled silica hollow spheres with controllable structures based on three-layer hybrid silica spheres. The void spacing between the shells can be tuned by manipulating the volume of TEOS and TSD added in each layer. The drug loading efficiency and release behavior of double-shelled silica hollow spheres were investigated by choosing mitoxantrone (Mito), an anti-cancer drug as a probing molecule. Green fluorescence labeled DSH@FITC was designed for evaluating *in vitro* cellular internalization of DSH. The *in vitro* study of Hep-G2 cells also proves that the DSH–Mito has enhanced therapeutic efficacy and no obvious adverse effect on cell viability.

Experimental

Chemicals and reagents

Tetraethoxysilane (TEOS), polyvinylpyrrolidone (PVP), cetyltrimethyl ammonium bromide (CTAB), sodium dodecyl sulfate (SDS), hydrofluoric acid (HF), sodium carbonate (Na_2CO_3), ammonia solution($NH_3 \cdot H_2O$) and ethanol (C_2H_5OH) were obtained from Sinopharm Chemical Reagent Beijing Co., Ltd. N-[3-(trimethoxysilyl)propyl] ethylenediamine (TSD) was purchased from Fluka. All reagents were used as received without any further purification.

Preparation of silica spheres with sandwich structure

The silica spheres with three layer sandwich structure (SSS) were fabricated *via* a modified Stöber reaction according to our previously reported method.[23] In a typical reaction, solution A (20 mL 1.5 mM TEOS in ethanol), solution B (20 mL 28% aqueous NH_3 and 60 mL ethanol) and solution C (6 mL 0.05 mM TSD in ethanol) were prepared. For fabricating the first layer, solution A was added dropwise into solution B for 12 min at a rate of 1 mL min^{-1} and reacted for 10 min under vigorous stirring to form the silica cores. For second layer, solution C and identical volume of TEOS were added into the reaction mixture synchronously, to form the middle layer of organic–silica framework. Lastly, for the third layer, remaining solution A was added to form the outer layer of silica shell. The adding of TEOS or TSD of the whole process was kept at the same rate. The reaction was kept for 3 h at 30 °C. The SSS were collected by centrifugation and washed with ethanol and water repeatedly.

Synthesis of single-shelled silica hollow spheres with acid etching

Single-shelled silica hollow spheres (SSH) were produced by etching the as-prepared SSS with 10% HF (aqueous). Briefly, a certain mount of 10% HF was added dropwise into SSH suspension (20 mL, 2 mg mL^{-1}), stirring for 10 min. The product was sufficiently washed repeatedly with water.

Synthesis of double-shelled silica hollow spheres with base etching

100 mg as-prepared SSH were added into 50 mL water solution containing 318 mg of Na_2CO_3 and 45.5 mg CTAB. After the reaction was stirred at 60 °C for 5 h, the double-shelled silica hollow spheres (DSH) were collected by centrifugation and washed with ethanol and water repeatedly. To avoid the toxicity of CTAB, the DSH were re-dispersed in 100 mL of acetone and refluxed at 80 °C for 48 h to remove the residual CTAB.

In vitro drug loading and release

20 mg of DSHs were dispersed in a solution of mitoxantrone (Mito) (10 mg mL^{-1} in water) and stirred for 24 h, followed by centrifugation and washing extensively to obtain the drug-loaded DSHs. For the drug release assay, the Mito loaded DSH samples were immersed into phosphate-buffered saline (PBS, pH of 5.0). The mixtures were centrifuged and the supernatant was extracted at given time intervals. The concentration of Mito was determined by UV-vis spectroscopy measurements using the absorption peak at 609 nm.

In vitro cellular internalization

Human liver carcinoma cells of Hep-G2 cells (ATCC) were maintained in high glucose Dulbecco's modified Eagle's medium (DMEM) (Gibco), supplemented with 10% FBS (Hyclone) at 37 °C in a humidified atmosphere of 5% CO_2. The cell culture media were supplemented with 100 units/mL penicillin and 100 g mL^{-1} streptomycin. The Hep-G2 cells were seeded on glass-bottom dishes (35 mm, MatTek Corporation). A final concentration of 100 μg mL^{-1} DSH@FITC was added to the cells and incubated for 4 h. Micrographs were taken on a Nikon fluorescence microscope (Nikon Eclipse Ti–S, CCD: Ri1). For co-localization with lysosome, the cells were co-incubated with 100 μg mL^{-1} of DSH@FITC for 4 h, and then washed, stained with 60 nM Lysotracker Red DND-99 (Beyotime Institute of Biotechnology, Haimen, China) for 1 h, and observed on a fluorescence microscope.

In vitro cytotoxicity

The cytotoxicity of DSH, DSH-Mito and free Mito was evaluated by WST-1 assay (WST-1 Cell Proliferation and Cytotoxicity Assay Kit). For 24 h detection, the cells were seeded at a density of 8000 cells/well on 96-well plates (Costar), and for 72 h

detection, the cell density was 2000 cells/well. After incubating the cells with DSH-Mito and free Mito for 24 h or 72 h, WST-1 solution was then added to cells and incubated for another 2 h. The absorbance of each well was measured at 450 nm *versus* a 630 nm reference on a scanning multiwell spectrometer (Multiskan MK3 Thermo labsystems).

Characterization

Transmission electron microscope (TEM) images were obtained using a JEM-2100F electron microscope, operating at 200 kV. Scanning electron microscopy (SEM) measurement was performed with a Hitachi S-4800 Scanning Electron Field Emission Microscope. The surface area was measured by the Brunauer–Emmett–Teller (BET) method using nitrogen adsorption and desorption isotherms on a Micrometrics ASAP 2020 system. The pore size distribution plot was obtained by the Barrett–Joyner–Halenda (BJH) method. UV-Vis absorbance spectra were recorded using a JASCO V-570 spectrophotometer at room temperature.

Results and discussion

Morphology and structure characterization

Fig. 1 illustrates the synthesis process of double-shelled silica hollow spheres. Silica spheres with sandwich structure were prepared first. Then, the single-shelled silica hollow spheres were fabricated by etching silica spheres with sandwich structure using hydrofluoric acid (HF). The middle layer was organic–inorganic hybrid structure co-condensed from TEOS and TSD and has less compact structure than the pure silica framework, HF as etchant has a tendency to selectively etch the middle layer of SSS. When these single-shelled silica hollow spheres were treated by Na_2CO_3 in the presence of CTAB in an appropriate concentration, the silica hollow spheres with double shell were successfully prepared.

Typical SEM and TEM images of silica spheres with sandwich structure (SSS-1), single-shelled silica hollow spheres (SSH-1) and double-shelled silica hollow spheres (DSH-1) are shown in Fig. 2. From the low-magnification SEM images, spherical particles with a narrow size distribution were observed, indicating a high yield of the silica nanospheres was obtained. Fig. 2a–c show SEM and TEM images of the hybrid silica spheres with a diameter of about 260 nm. The spheres are significantly monodispersed and uniform. From Fig. 2d–f, it can be seen that the single-shelled silica hollow spheres have uniform shell thickness (*ca.* 25 nm) and core diameter (*ca.* 190 nm), and the diameters (*ca.* 260 nm) have not obviously changed compared with that of hybrid silica spheres. The morphology and structure of double-shelled silica hollow spheres are shown in Fig. 2g–i. The double-shelled hollow structure of the spheres was confirmed from the high-magnification TEM image shown in Fig. 2i. It can be clearly observed that the DSH has two shells. The thickness of inner shell is approximate 25 nm. The outer shell of the DSH-1 is about 20 nm in thickness. The size of whole sphere is about 260 nm and the void is about 100 nm in diameter. Nitrogen adsorption–desorption isotherms of SSH-1 and DSH-1 were measured to determine the specific surface area and pore size, and the corresponding results are shown in Fig. 3. The Brunauer–Emmett–Teller (BET) surface area of single-shelled silica hollow spheres calculated from the desorption branch of the isotherm pore volume were 45.8 $m^2\ g^{-1}$. For the double-shelled silica hollow spheres, the BET surface area was increased to 121.7 $m^2\ g^{-1}$. The corresponding pore size distributions are shown in the inset of Fig. 3, the average Barrett–Joyner–Halenda (BJH) pore diameter of single-shelled silica hollow spheres is determined to be 2.1 nm. For double-shelled silica hollow spheres, average pore size increased to 2.8 nm. Based on TEM images, the larger pores are believed to result from the shells that have been etched extensively.

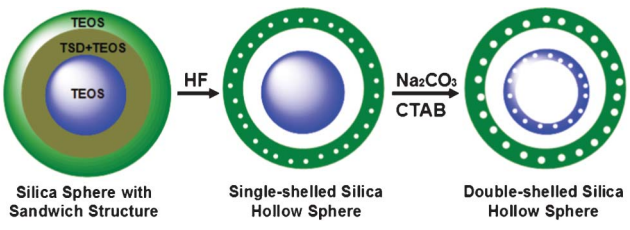

Fig. 1 Schematic illustration of the formation procedure of double-shelled silica hollow spheres.

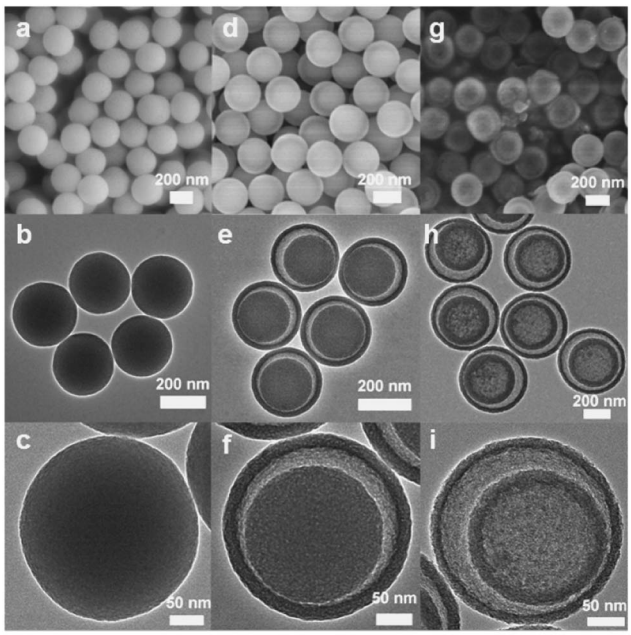

Fig. 2 SEM and TEM images of silica spheres with sandwich structure (a, b, c), single-shelled silica hollow spheres (d, e, f) and double-shelled silica hollow spheres (g, h, i).

Tuning the inner space of double-shelled silica hollow spheres

By changing the composition of three-layer organic–inorganic hybrid silica spheres, the void spacing of double-shelled silica hollow spheres can be tuned. Keeping the total volume of TEOS unchanged, the silica inner core of single-shelled hollow spheres decreases with reducing the adding volume of TEOS in

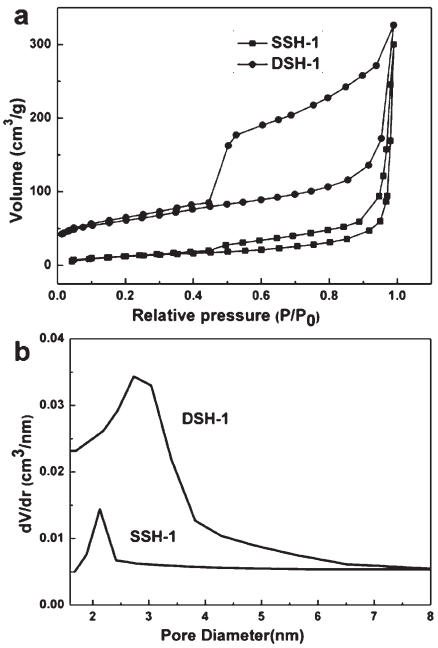

Fig. 3 Nitrogen adsorption–desorption isotherms (a) and pore size distribution (b) of single-shelled silica hollow spheres and double-shelled silica hollow spheres.

the first layer and increasing the volume of TSD and TEOS in second layer. As shown in Fig. 4a, the silica inner core of single-shelled hollow spheres was about 110 nm, which was fabricated by using 8 mL TEOS in the first layer and 10 mL TSD in the second layer. Reducing the volume of TEOS in the first layer to 4 mL and increasing the volume of TSD in the second layer to 14 mL will decrease the diameter of silica inner core to 70 nm, shown in Fig. 4d. After treated by Na_2CO_3 in the presence of CTAB, the single-shelled hollow spheres were transferred to double-shelled silica hollow spheres with different shell-to-shell distances (Fig. 4b,c,e,f). Tuning the inner void and shell-to-shell distance is promising for applications requiring selective transportation of molecules through the shell.

Formation mechanism of double-shelled silica hollow spheres

To investigate the formation mechanism of the double-shelled silica hollow spheres, time-dependent experiments were carried out. The synthesis process of double-shelled hollow spheres at different reaction time were monitored and characterized by TEM. At the beginning stage of the reaction, the silica inner core begun to dissolve, which was etched by Na_2CO_3. The dissolved silica species were absorbed and re-deposited on the outer shell assisting by CTAB, shown in Fig. 5a and 5b. The re-deposited silica species and CTAB protect the shell from etching by Na_2CO_3. With the increasing of the reaction time, the dissolution and re-deposition of silica proceed simultaneously to yield the hollow space in the inner silica core. As the etching time is prolonged to 4 h, the double shell was formed and the re-deposited silica species on the outer shell begun to dissolve (Fig. 5c and 5d). After etching for a total of 6 h, the double-shelled silica hollow spheres with smooth shell were prepared, shown in Fig. 2g–i. Based on the observation of the etching experiments, four important processes are proposed during the formation of the double-shelled hollow spheres. (1) Adsorption of CTAB on the surface of single-shelled silica hollow spheres, (2) slow dissolution of silica inner core to form soluble silicate species, (3) absorption and re-deposition of silicate species on the shell assisting by CTAB, (4) dissolution of silicate species on the shell and formation of double-shelled silica hollow spheres.

To understand the important role of the CTAB in the formation of double-shelled silica hollow spheres, comparative experiments were carried out by etching single-shelled silica hollow spheres without CTAB or replacing CTAB with other surfactants. As shown in Fig. 6a and b, in the absence of CTAB, the outer shells of single-shelled silica hollow spheres were almost etched away and the silica inner cores were transferred

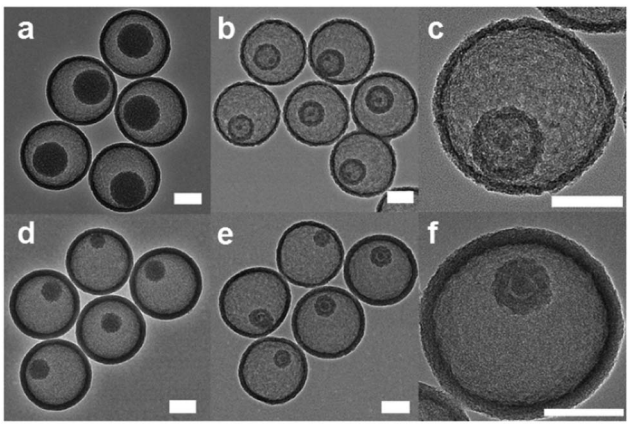

Fig. 4 TEM images of single-shelled silica hollow spheres with medium core (a) and double-shelled silica hollow spheres with medium void (b, c), and single-shelled silica hollow spheres with small core (d) and double-shelled silica hollow spheres with large void (e, f). All scale bars are 100 nm.

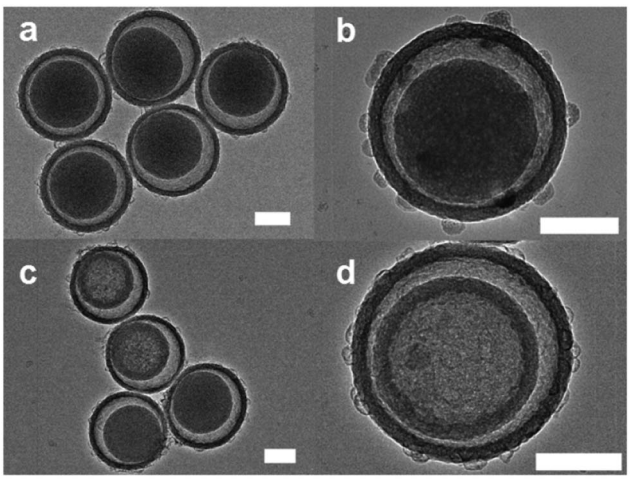

Fig. 5 TEM images of single-shelled silica hollow spheres etched by Na_2CO_3 in the presence of CTAB at different time (a, b): 2 h, (c, d): 4 h during the etching process. All scale bars are 100 nm.

to hollow structure. This observation indicated that CTAB added in the reaction system protects the shell from etching by Na_2CO_3. If the CTAB was replaced with SDS, similar phenomenon was observed (Fig. 6c and d). If the CTAB was replaced with PVP, the outer shells were etched away and only a few of silica inner cores were transferred to hollow structure (Fig. 6e and f). The added PVP may affect the etching of silica inner cores by Na_2CO_3. Therefore, in our work, the CTAB play important roles in protecting the shell from etching and selectively etching silica inner cores by Na_2CO_3.

In vitro drug storage and release

Because of the high specific surface area and hierarchical nanostructures, the multi-shelled silica hollow spheres have great potential in the application of drug delivery. Yin *et al.* demonstrate the unique drug delivery profile of SiO_2@void@SiO_2 by using R6G as a model molecule. Yeh *et al.* also comparatively studies the release properties between double-shelled and triple-shelled nanospheres by using FITC fluorophore as a model. To make a further progress for the drug delivery, we choose a typical anti-cancer drug, mitoxantrone (Mito) as a probing drug to investigate the drug loading capacity and release properties of silica hollow spheres with single shell or double-shell. Mito has been widely used for the treatment of breast and prostate cancer but the severe heart toxicity limits its clinical application. Liposomes, polymer nanoparticles, mesoporous silica nanoparticles (MSN) have been reported to improve Mito formulation and reduce the inherent toxicity of Mito.[27–30] But the drug loading capacity and release rate needed to be improved. In this work, the loading capacities of Mito were measured to be 193 mg and 405 mg per g SiO_2 for SSH-1 and DSH-1. DSH-1 has an obvious higher drug loading capacity, which is attributed to its higher BET specific surface area, the pore size, larger inner cavity and their unique mesoporous structures and hollow cavity. Fig. 7 shows the cumulative drug release of Mito from the SSH-1 and DSH-1 at pH of 5.0 and physiological temperature. The kinetic release curves were calculated by using the absorption of the peak at 609 nm. The Mito concentration gradually increases with prolonging of time, indicating sustained release of Mito molecules. The Mito amounts released from double-shelled silica hollow spheres with large silica inner core reach about 80% in 6 days. It exhibited a low initial burst release (within 20% of the loaded amount) within 2 h and a two-phase drug release behavior. The initial rapid release rate in 0–20 h was attributed to the drugs interacting on the outside shell of the DSH, and further sustained release with a lower release rate from 20 h to 8 days was attributed to the drugs being located in the inner shell and the hollow space of the DSH.

In vitro cellular internalization

Efficient cellular internalization of nanoparticles is necessary for intracellular drug delivery and efficient therapy. To monitor the trafficking of DSH intracellularly, luminescent labeled DSH@FITC with green fluorescence was designed and synthesized by incorporating the fluorescent dye of fluorescein isothiocyanate into the inner shell of the DSH. The preparation of DSH@FITC is similar to DSH except adding an amount of FITC to form the silica core. The size and morphology is the same as DSH. The uptake of DSH@FITC by human liver carcinoma cell of Hep-G2 was evaluated by fluorescence microscopy. The Hep-G2 cells were incubated with 100 μg mL^{-1} of DSH@FITC for 4 h and then stained with Lysotracker Red DND-99 to label the lysosomes. From the green

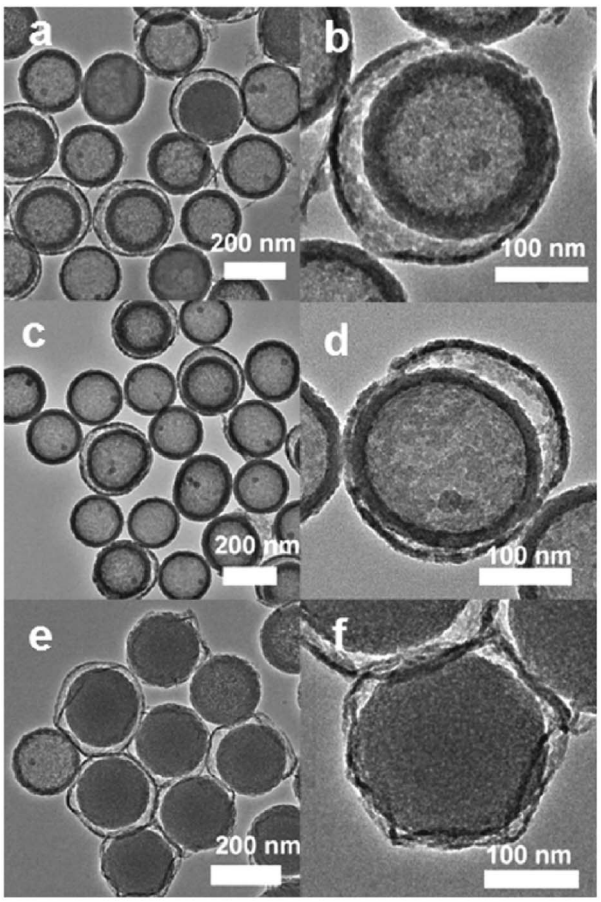

Fig. 6 TEM images of single-shelled silica hollow spheres etched by Na_2CO_3 in the absence of CTAB (a, b), and in the presence of SDS (c, d) and PVP (e, f). All scale bars are 200 nm.

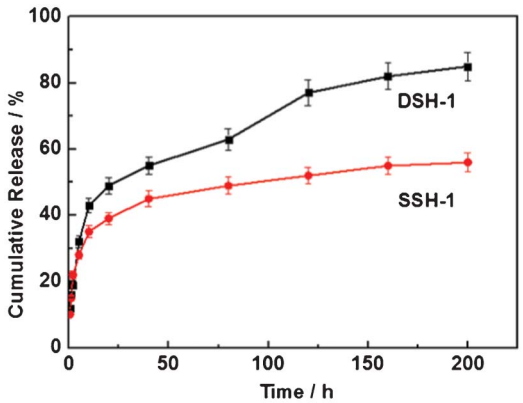

Fig. 7 The cumulative drug release of Mito from the SSH-1 and DSH-1 at pH of 5.0 and physiological temperature.

fluorescence in Fig. 8a, it is seen that DSH@FITC distributed in almost all of the cells throughout the entire cell cytoplasm. The co-localization between DSH@FITC (green) and lysosome (red fluorescence, Fig. 8b) shows that the part of DSH@FITC has escaped from the lysosome to the cytosol. This behavior may be attributed to the "proton sponge" effect and is important for endosome escape.[26,31] Therefore, DSHs are helpful for increasing the cell internalization, decreasing the drug efflux, and increasing the intracellular accumulation of the drugs.

In vitro cytotoxicity

The cytotoxic effect of the DSH–Mito was evaluated and compared with free Mito *via* the WST-1 assay. As shown in Fig. 9a,b, the cytotoxic efficacy of the DSH–Mito and free Mito against Hep-G2 cells increased with an increase in their concentrations from 0.625 to 10 μg mL^{-1}. After they were cultured together for 24 h, DSH–Mito induced Hep-G2 cell death comparable to free Mito. After they were cultured together for 72 h, the DSH–Mito exhibited obvious greater cytotoxicity than free Mito in all concentrations except for 0.625 μg mL^{-1}. It is speculated that the increased cytotoxicity of DSH–Mito over free Mito is mainly due to the sustained release of the drug molecules from the double-shelled silica nanorattles and contributed from enhanced Mito uptake by cells when they loaded in DSH. The biocompatibility of intact DSH was also detected. Various concentrations of DSH were incubated for 24 h and 72 h with Hep-G2 and then cell viability was assessed. Within the tested concentration range even as high as 400 μg mL^{-1}, the DSH has no obvious adverse effect on cell viability, demonstrating the DSH itself has no cytotoxicity (Fig. 9c,d).

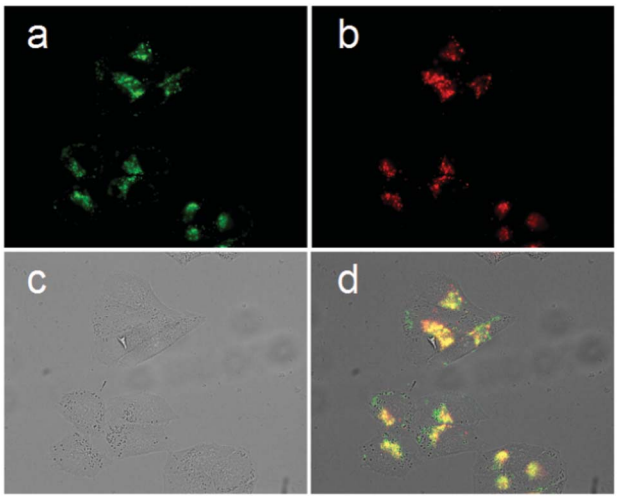

Fig. 8 Fluorescence microscopy images showing the internalization of DSH@FITC. (a) Green fluorescence shows the location of DSH@FITC. (b) Red fluorescence shows the location of lysosome (Lysotracker Red DND-99). (c) Corresponding transmission image. (d) Overlaid image of a, b and c.

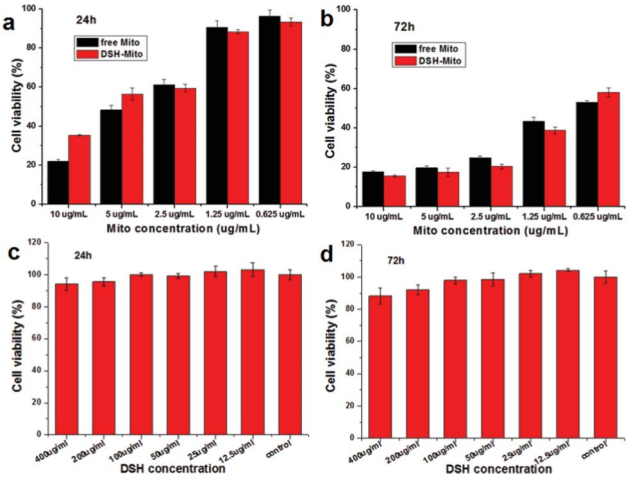

Fig. 9 Comparison of the cytotoxic effects of different delivery modes of Mito in Hep-G2 cells at different concentrations for 24 h (a) and 72 h (b). The cytotoxic effects of DSH on cell viability evaluated by incubating various concentrations of DSH for 24 h (c) and 72 h (d) with Hep-G2.

Conclusions

In conclusion, we have developed an alternating acid/base selective etching strategy to synthesize double-shelled silica hollow spheres. The uniformity, mono-disperse, shells and inner space of hollow spheres were well controlled. Drug delivery of anti-cancer drug Mito showed that these double-shelled silica hollow spheres have a high drug loading capacity and exhibit sustained release of drug compared with conventional single-shelled silica hollow spheres due to their hierarchically mesoporous structures. The *in vitro* cellular internalization of DSH was evaluated by designing luminescent labeled DSH@FITC with green fluorescence. *In vitro* cytotoxicity show that DSH has no obvious adverse effect on cell viability and the DSH is an ideal carrier for drug delivery. Given the versatility of this strategy, it will have great potential to fabricate multifunctional hollow spheres with hierarchical nanostructures and complex compositions, such as multifunctional magnetic drug carriers for targeting, MRI imaging and hyperthermia for cancer therapy.[32–36]

Acknowledgements

This work was supported by the National Natural Science Foundation of China (No. 51202260, 81201814, 81171454 and 31271075).

Notes and references

1 X. W. Lou, L. A. Archer and Z. C. Yang, *Adv. Mater.*, 2008, **20**, 3987–4019.
2 Y. Zhao and L. Jiang, *Adv. Mater.*, 2009, **21**, 3621–3638.
3 J. Liu, S. Z. Qiao, J. S. Chen, X. W. Lou, X. R. Xing and G. Q. Lu, *Chem. Commun.*, 2011, **47**, 12578–12591.

4 F. Q. Tang, L. L. Li and D. Chen, *Adv. Mater.*, 2012, **24**, 1504–1534.
5 H. Y. Liu, D. Chen, L. L. Li, T. L. Liu, L. F. Tan, X. L. Wu and F. Q. Tang, *Angew. Chem., Int. Ed.*, 2011, **50**, 891–895.
6 L. F. Tan, D. Chen, H. Y. Liu and F. Q. Tang, *Adv. Mater.*, 2010, **22**, 4885–4889.
7 W. Li, Y. H. Deng, Z. X. Wu, X. F. Qian, J. P. Yang, Y. Wang, D. Gu, F. Zhang, B. Tu and D. Y. Zhao, *J. Am. Chem. Soc.*, 2011, **133**, 15830–15833.
8 L. J. Han, R. J. Liu, C. S. Li, H. H. Li, C. X. Li, G. J. Zhang and J. N. Yao, *J. Mater. Chem.*, 2012, **22**, 17079–17085.
9 X. Y. Lai, J. Li, B. A. Korgel, Z. H. Dong, Z. M. Li, F. B. Su, J. A. Du and D. Wang, *Angew. Chem., Int. Ed.*, 2011, **50**, 2738–2741.
10 S. L. Xiong and H. C. Zeng, *Angew. Chem., Int. Ed.*, 2012, **51**, 949–952.
11 M. Yang, J. Ma, C. L. Zhang, Z. Z. Yang and Y. F. Lu, *Angew. Chem., Int. Ed.*, 2005, **44**, 6727–6730.
12 L. Zhou, D. Y. Zhao and X. W. Lou, *Adv. Mater.*, 2012, **24**, 745–748.
13 C. F. Zhang, H. B. Wu, C. Z. Yuan, Z. P. Guo and X. W. Lou, *Angew. Chem., Int. Ed.*, 2012, **51**, 9592–9595.
14 Q. Zhang, J. P. Ge, J. Goebl, Y. X. Hu, Z. D. Lu and Y. D. Yin, *Nano Res.*, 2009, **2**, 583–591.
15 C. C. Huang, W. Huang and C. S. Yeh, *Biomaterials*, 2011, **32**, 556–564.
16 X. J. Wu and D. S. Xu, *Adv. Mater.*, 2010, **22**, 1516–1520.
17 J. Liu, S. B. Hartono, Y. G. Jin, Z. Li, G. Q. Lu and S. Z. Qiao, *J. Mater. Chem.*, 2010, **20**, 4595–4601.
18 G. L. Li, Q. Shi, S. J. Yuan, K. G. Neoh, E. T. Kang and X. L. Yang, *Chem. Mater.*, 2010, **22**, 1309–1317.
19 X. B. Li, X. Liu, Y. Ma, M. R. Li, J. Zhao, H. C. Xin, L. Zhang, Y. Yang, C. Li and Q. H. Yang, *Adv. Mater.*, 2012, **24**, 1424–1428.
20 X. L. Huang, X. Teng, D. Chen, F. Q. Tang and J. Q. He, *Biomaterials*, 2010, **31**, 438–448.
21 N. J. Hao, L. L. Li, Q. Zhang, X. L. Huang, X. W. Meng, Y. Q. Zhang, D. Chen, F. Q. Tang and L. F. Li, *Microporous Mesoporous Mater.*, 2012, **162**, 14–23.
22 H. Y. Liu, T. L. Liu, L. L. Li, N. J. Hao, L. F. Tan, X. W. Meng, J. Ren, D. Chen and F. Q. Tang, *Nanoscale*, 2012, **4**, 3523–3529.
23 D. Chen, L. L. Li, F. Q. Tang and S. O. Qi, *Adv. Mater.*, 2009, **21**, 3804–3807.
24 F. G. Gao, L. L. Li, T. L. Liu, N. J. Hao, H. Y. Liu, L. F. Tan, H. B. Li, X. L. Huang, B. Peng, C. M. Yan, L. Q. Yang, X. L. Wu, D. Chen and F. Q. Tang, *Nanoscale*, 2012, **4**, 3365–3372.
25 L. L. Li, F. Q. Tang, H. Y. Liu, T. L. Liu, N. J. Hao, D. Chen, X. Teng and J. Q. He, *ACS Nano*, 2010, **4**, 6874–6882.
26 L. L. Li, Y. Q. Guan, H. Y. Liu, N. J. Hao, T. L. Liu, X. W. Meng, C. H. Fu, Y. Z. Li, Q. L. Qu, Y. G. Zhang, S. Y. Ji, L. Chen, D. Chen and F. Q. Tang, *ACS Nano*, 2011, **5**, 7462–7470.
27 Y. H. Ma, L. Zhou, H. Q. Zheng, L. Xing, C. G. Li, J. H. Cui and S. A. Che, *J. Mater. Chem.*, 2011, **21**, 9483–9486.
28 A. Wani, E. Muthuswamy, G. H. L. Savithra, G. Z. Mao, S. Brock and D. Oupicky, *Pharm. Res.*, 2012, **29**, 2407–2418.
29 S. L. Law, C. K. Ho, T. F. Jang, P. Chang and F. M. Lin, *Int. J. Pharm.*, 1996, **128**, 139–143.
30 H. L. Chen, W. Z. Yang, H. Chen, L. R. Liu, F. P. Gao, X. D. Yang, Q. Jiang, Q. Q. Zhang and Y. S. Wang, *Colloids Surf., B*, 2009, **73**, 212–218.
31 O. Boussif, F. Lezoualc'h, M. A. Zanta, M. D. Mergny, D. Scherman, B. Emeneix and J. P. Behr, *Proc. Natl. Acad. Sci. U. S. A.*, 1995, **92**, 7297–7301.
32 W. R. Zhao, H. R. Chen, Y. S. Li, L. Li, M. D. Lang and J. L. Shi, *Adv. Funct. Mater.*, 2008, **18**, 2780–2788.
33 Y. Chen, H. R. Chen, M. Ma, F. Chen, L. M. Guo, L. X. Zhang and J. L. Shi, *J. Mater. Chem.*, 2011, **21**, 5290–5298.
34 Y. Hu, X. T. Zheng, J. S. Chen, M. J. Zhou, C. M. Li and X. W. Lou, *J. Mater. Chem.*, 2011, **21**, 8052–8056.
35 H. X. Wu, G. Liu, S. J. Zhang, J. L. Shi, L. X. Zhang, Y. Chen, F. Chen and H. R. Chen, *J. Mater. Chem.*, 2011, **21**, 3037–3045.
36 H. S. Cho, Z. Y. Dong, G. M. Pauletti, J. M. Zhang, H. Xu, H. C. Gu, L. M. Wang, R. C. Ewing, C. Huth, F. Wang and D. L. Shi, *ACS Nano*, 2010, **4**, 5398–5404.